AIAA AVIATION Forum
13-17 June 2016, Washington, D.C.
46th AIAA Thermophysics Conference

10.2514/6.2016-4021

Vibrational relaxation and dissociation in O_2–O mixtures

Daniil A. Andrienko* Kevin Neitzel†

Iain D. Boyd ‡

Department of Aerospace Engineering, University of Michigan, Ann Arbor, MI, 48109

Thermal relaxation in O_2–O mixtures is studied using state-specific transition rate coefficients, generated by extensive trajectory simulations. Both O_2–O and O_2–O_2 collisions are concurrently simulated in the evolving nonequilibrium gas mixture under constant heat bath conditions and in one-dimensional shock flow. Accuracy of the state-resolved and multi-temperature models is assessed by comparing computed temperatures and atomic oxygen number density with experimental data. The effect of rotational nonequilibrium is included to provide a realistic description of the energy balance in strong shock waves. The present study demonstrates the importance of atom-diatom collisions due to the extremely efficient energy randomization in the intermediate O_3 complex. It is shown that the presence of atomic oxygen has a significant impact on vibrational relaxation time at temperatures observed in hypersonic flow. The population of highly-excited O_2 vibrational states is affected by the amount of atomic oxygen when modeling the relaxation under constant heat bath conditions. Recommendations on accuracy of the low fidelity thermochemistry models of oxygen are provided.

I. Introduction

Hypersonic flight experiments, conducted during the past several decades, have revealed a necessity of coupling the experimental and theoretical approaches in order to improve the existing computational models of nonequilibrium air plasma. One of the important aspects of hypersonic aerothermodynamics is the energy exchange among the translational and internal degrees of freedom (DOF) of species behind a shock wave. Since the characteristic times of excitation of translational and vibrational modes differ by orders of magnitude, the hypersonic flow can be in a state of thermal nonequilibrium. Furthermore, the excitation of internal DOF is coupled to the dissociation process. Thus, it is important to accurately model the energy exchange in order to predict the structure of the shock wave.

Among other phenomena that take place in shock waves, the vibrational excitation and deactivation play an important role in the energy balance. For the past decade, a significant improvement in the fidelity of existing models of air species has been accomplished. Most of the progress has been achieved in modeling of molecular nitrogen [1–3], because of its importance in re-entry flows.

Systems that contain oxygen are studied less often, mainly because oxygen quickly dissociates in a strong shock wave [4–7]. However, a significant amount of molecular oxygen is observed during hypersonic cruise flight in the post-shock region. This flight regime is inherent in hypersonic vehicles which travel at a speed of about 2–3 km/s. The vibrational relaxation in O_2–O collisions is known to proceed several orders of magnitude faster than in other types of collisions in air and does not follow the conventional dependence on temperature of the gas flow [8]. These factors make a SR kinetic approach a very desirable technique, since it is possible to model thermal nonequilibrium in shock and expanding flows without invoking the thermodynamic definition of temperature.

The state-specific transition rates in O_2–O collisions were recently computed [9, 10] on the accurate, many-body potential energy surface [11] using the Quasi Classical Trajectory (QCT) method. These rates,

*Postdoctoral research fellow, Department of Aerospace Engineering, University of Michigan, 1320 Beal Ave
†PhD candidate, Department of Aerospace Engineering, University of Michigan, 1320 Beal Ave
‡James E. Knott Professor, Department of Aerospace Engineering, University of Michigan, 1320 Beal Ave

employed in the master equation simulation [12], revealed an anomalously fast vibrational relaxation time in atom-diatom collisions, compared to other molecular systems containing oxygen. These findings were related to the existence of a large attractive component in the O_3 PES that leads to an extremely efficient energy randomization.

The state-resolved (SR) kinetic models are of significant interest due to their accuracy in describing the nonequilibrium flows over the large range of input parameters. These models are applied to describe kinetics of hypersonic flow in shock waves [13, 14], nozzle flow [15] and in boundary layers [16]. Under nonequilibrium conditions, the population of the vibrational manifold can be appreciably different from the equilibrium distribution. In shock waves, highly energetic vibrational states are underpopulated and dissociative reactions are dominant. The multi-temperature (MT) model is the alternative to the SR models for describing shock flows with the vibrational temperature less than the translational one. However, when the opposite situation takes place, i.e. the flow cools down, the selective recombination pumps energy into high vibrational states, forming the long plateau of the vibrational distribution. The multi-temperature model is not adequate in this regime since the global chemical rates exhibit strong non-Arrhenius behavior. The rates of dissociation in strongly recombining flow are related to either the atomic concentration or to the population of last vibrational state rather than to the vibrational temperature. A comprehensive investigation of N_2/N cooling flows was performed by Colonna and coworkers [17, 18]. In the present work, some insight on O_2/O recombinative flow is obtained by implementing the present O_2–O rates.

In order to bring the present simulation closer to real conditions, O_2–O_2 collisions are included as well. The atom-diatom and diatom-diatom collisions are simultaneously modeled in the present work. Because an accurate trajectory simulation of bimolecular collisions in oxygen gas is yet to be conducted, the Forced Harmonic Oscillator (FHO) model [19] is employed to obtain the O_2–O_2 vibration-translation (VT) and vibration-vibration (VV) transition rates. To model the SR O_2–O_2 dissociation, several techniques are employed in the present paper. First, the SR QCT calculations using the O_4 Varandas PES are conducted. These bound-free (BF) rate coefficients (RC) are compared to the $O_2(v)$–O_2 BF RCs obtained via the scaling procedure from O_2–O state-specific QCT data. The third approach employs the concept of preferential dissociation [20] to generate the $O_2(v)$–O_2 BF RCs. The accuracy of these methods is assessed by comparing computed and experimental values of species number density.

This paper is organized as follows. Section II provides details on O_2–O collisions, and addresses the main features of the master equations and multi-temperature models. The detailed study of vibrational relaxation and dissociation in oxygen gas is presented in Section III. Vibration-to-translation transition rates and corresponding relaxation times are discussed in Section III.A. Importance of multiquantum transitions in heating and cooling flows is discussed in Section III.B. Dissociation and recombination processes are studied in Section III.C. The comparison of SR and MT thermodynamic models is performed in Section III.D for heat bath conditions. A similar discussion for shock flows is given in Section III.E. Conclusions are provided in Section IV.

II. Governing equations

A. Specifics of O_2–O collisions

The O_2–O vibration-to-translation (VT) transition rates, employed in the present work, are obtained on the accurate potential energy surface by [11] using the Quasi-Classical Trajectory (QCT) method [21]. The Varandas PES generates 47 vibrational levels and a maximum of 236 rotational levels for molecular oxygen in the ground electronic state. The total number of rovibrational levels in the ground electronic state of oxygen is 6,245, however, taking into account the nuclear spin statistics of a homonuclear molecule, the even numbered rotational levels for the $O_2(X^3\Sigma_g^-)$ state are forbidden. Since, during a bound-bound rovibrational transition, the symmetry of the initial and final states cannot change, transitions of the O_2 molecule in the ground electronic state are only allowed between odd–numbered rotational levels [22]. The energies of rovibrational states are calculated by the WKB approach.

The cross sectional data of bound-bound transitions, generated by the QCT method [23], is modified to take into account the degeneracy of the spin and orbital momentum of reactants. The degeneracy factor of the $O(^3P)$ and $O_2(^3X_g^-)$ reactants can be expressed in the form, given by [24]:

$$\frac{1}{g_{BB}} = 3\left(5 + 3exp\left(-\frac{227.6}{T}\right) + exp\left(-\frac{325.9}{T}\right)\right) \quad (1)$$

The degeneracy factor of the bound-bound transition is found as a ratio of the PES degeneracy to the degeneracy of the reactants. Taking into account that the present O_3 PES is non-degenerate, the total degeneracy for the reaction of bound-bound transitions is given by Eq. (1). At high temperatures, the degeneracy factor asymptotically approaches a factor of 1/27. This means that the reaction takes place on only one of the 27 possible potential energy surfaces.

The dissociation of molecular oxygen in a shock wave with a temperature above a few thousands of K is unlikely to proceed in the adiabatic manner. One way to account for alternative channels of dissociation from excited electronic states is to assume equilibrium between lower vibrational levels of the excited electronic state and high vibrational levels of the ground state [25]. The contribution of dissociation from the excited electronic level should be added to the dissociation rate from the ground electronic level. It is possible to calculate the degeneracy factor of the dissociation reaction for each rovibrational level of the ground electronic state individually [26]. In this case, the degeneracy is calculated by assuming only electronic levels with a minimum of energy below the energy of the current rovibrational level. The degeneracy of the bound-free transition for the rovibrational level (v, j) is then computed as follows:

$$g_{BF,\nu,j} = 1 + \frac{\sum g^E}{g^X}, \tag{2}$$

where $g^X = 3$ is the degeneracy of the ground electronic state, and g^E is the degeneracy of the electronically excited state. The assumption of equilibrium between the vibrational levels of the ground and excited states is valid if the following condition holds:

$$e^X_{\nu,j} > e^E_{\nu=0,j=0}. \tag{3}$$

Assuming that Eq. (3) holds for every rovibrational level of the ground electronic state, one can obtain the degeneracy factor of the bound-free transition, originally proposed in [25]: $g_{BF} = 16/3$.

The vibration-to-translation and vibration-to-vibration (VV) transition rates in O_2–O_2 collisions are obtained by means of the FHO model [19]. In order to generate the state-specific VT and VV transition rates the following parameters of the O_2–O_2 system are used: $\alpha = 4.2$ Å^{-1} and $d = 3.75$ Å, where α describes the steepness of a purely repulsive intermolecular potential $V(r) \sim exp(-\alpha r)$ and d is the hard sphere diameter of oxygen. Because the probability of multiquantum jumps in the O_2–O_2 system is much lower than that with $|\Delta v| = 1$, only transitions with $|\Delta v| \leq 5$ are considered in the present work. The database of O_2–O rates, employed in the present work, includes all possible transitions [23].

B. Master equations

The preliminary study of vibrational relaxation of oxygen includes only the bound-bound transitions in a system of master equations. Because at moderate temperatures (below 10,000 K) the trans-rotational equilibrium in hypersonic flows occurs much faster than the trans-vibrational one, the former is assumed throughout the present paper. This step significantly reduces the number of equations to be solved. The resulting equation for the number density of vibrational level i can be written as follows:

$$\frac{dn_i}{dt} = \sum_{i' \neq i} \left(K^{O_2-O}_{i' \to i} n_O n_{i'} - K^{O_2-O}_{i \to i'} n_O n_i \right) + \sum_{i' \neq i} \left(K^{O_2-O_2}_{i' \to i} n_{O_2} n_{i'} - K^{O_2-O_2}_{i \to i'} n_{O_2} n_i \right)$$
$$\sum_m \sum_{m'} \sum_{i'} \left(Q^{m \to m'}_{i \to i'} n_i n_m - Q^{m' \to m}_{i' \to i} n_{i'} n_{m'} \right), \; i = 1 ... N_v, \tag{4}$$

where $K^{O_2-O}_{i' \to i}$ and $K^{O_2-O_2}_{i' \to i}$ are the VT bound-bound transition rates in O_2–O and O_2–O_2 collisions, respectively, $Q^{m' \to m}_{i' \to i}$ is the VV RC of the reaction $O_2(m) + O_2(i) \to O_2(m') + O_2(i')$, and N_v is the total number of vibrational states. An implicit method is applied to integrate Eq. (4) with third order accuracy for diagonal and second order accuracy for off-diagonal elements. The initial number density of rovibrational level i, j is evaluated as follows:

$$n^0_{i,j} = \frac{Q_{i,j}}{\sum_i Q_{i,j}} n^0_{O_2}, \tag{5}$$

where $Q_{i,j} = (2j+1)\, exp(-e_{i,0}/kT_v) \times exp(-(e_{i,j} - e_{i,0})/kT_r)$ is the rovibrational factor of level (i, j). The initial number density of vibrational level i is calculated as a sum of number densities of rotational levels

j, compatible with i. To reduce influence of statistical error of the QCT method, the principle of detailed balance is invoked to generate rates of exothermic transitions:

$$K_{i,j\to i',j'}Q_{i,j} = K_{i',j'\to i,j}Q_{i',j'}. \tag{6}$$

In order to verify the VT and VV rates, the system of master equations is solved assuming only bound-bound transitions in pure molecular oxygen under constant heat bath conditions with temperatures between 1,000 and 30,000 K. The comparison of resulting vibrational relaxation time and the experimental data is provided in section III. In the present work, the vibrational relaxation process is studied for different compositions of O_2 and O mixtures. In order to obtain the vibrational relaxation time in pure molecular oxygen, only terms in the second parentheses and the VV relaxation term in Eq. (4) are considered. The terms in the first parentheses are considered if only the O_2–O relaxation is of interest. Finally, all terms are taken into account if the relaxation is modeled in the presence of both O_2 and O projectiles.

The master equation in the presence of dissociation and recombination processes has the following appearance:

$$\begin{aligned}\frac{dn_i}{dt} = \sum_{i'\neq i}\left(K^{O_2-O}_{i'\to i}n_O n_{i'} - K^{O_2-O}_{i\to i'}n_O n_i\right) + \sum_{i'\neq i}\left(K^{O_2-O_2}_{i'\to i}n_{O_2} n_{i'} - K^{O_2-O_2}_{i\to i'}n_{O_2} n_i\right) + \\ \sum_m\sum_{m'}\sum_{i'}\left(Q^{m\to m'}_{i\to i'}n_m n_i - Q^{m'\to m}_{i'\to i}n_{i'} n_{m'}\right) + \\ R^{O_2-O_2}_i n_{O_2} n_O^2 - D^{O_2-O_2}_i n_{O_2} n_{O_2} + R^{O_2-O}_i n_O^3 - D^{O_2-O}_i n_{O_2} n_O,\ i = 1...N_\nu\end{aligned} \tag{7}$$

where $D^{O_2-O_2}_i$, $D^{O_2-O}_i$, $R^{O_2-O_2}_i$ and $R^{O_2-O}_i$ are the state-specific dissociation and recombination rates in O_2–O_2 and O_2–O collisions. The number density of atomic oxygen is given by the following equation:

$$\frac{dn_O}{dt} = \sum_i D^{O_2-O_2}_i n_i n_{O_2} - \sum_i R^{O_2-O_2}_i n_i n_O^2 + \sum_i D^{O_2-O}_i n_i n_O - \sum_i R^{O_2-O}_i n_O^3 \tag{8}$$

The rates of bound-bound and bound-free transitions can be averaged over the range of trans-rotational temperatures, since this type of thermal equilibrium is typically observed in gas flows with temperatures below 10,000 K. The system of master equations that employs rotationally-averaged RCs is termed as the VT model. Otherwise, when a complete set of rovibrationally resolved RCs is utilized, the system of master equations is termed as the RVT model.

C. State-specific dissociation rates

An important aspect of coupling the dissociation and thermal relaxation processes is the accurate state-specific O_2 dissociation rates in molecule-molecule and molecule-atom collisions. For the latter, accurate data is available for all internal states, obtained via the QCT method [10]. However, a complete database of O_2–O_2 transition rates is not yet available.

One of possible ways to estimate D_i in O_2–O_2 collisions is based on the fact that the dissociation rates in O_2–O collisions are weakly dependent on the attractive part of the potential energy surface and only affected by its repulsive branch. In [27], two potential energy surfaces were adopted: the first PES was obtained by the summation of the pairwise interactions in the O_2–O complex, described by the Hulburt–Hirshfelder (HH) potential [28]. The second PES accounted for the three-body interaction [11], in addition to the two-body term, included in the HH PES.

The comparison of these two approaches revealed a very small difference in dissociation rates, which indicates a minor influence of the three-body interaction term. Indeed, the dissociation process occurs at high collisions energies, when colliding particles interact mostly via the repulsive branch of the potential.

Thus, it appears reasonable to scale the accurate SR O_2–O dissociation RCs in order to obtain the BF transition RCs for the O_2–O_2 system. In the present work, the scaling factor is calculated as the ratio of the global dissociation RC for atom-diatom and diatom-diatom collisions. The state-specific O_2–O_2 dissociation RCs are calculated as follows:

$$D^{O_2-O_2}_i = D^{O_2-O}_i \frac{D^{O_2-O_2}}{D^{O_2-O}},\ i = 1...N_v. \tag{9}$$

Source	$A, cm^3/s$	B	C, K
Camac, 1961	5.978×10^{-5}	-1.00	59415
Johnston, 1968	4.980×10^{-6}	-1.00	59500
Bortner, 1969	1.370×10^{-5}	-0.83	59400
Park, 1989	3.320×10^{-3}	-1.50	59500
Ibraguimova et al., 2003	1.627×10^{1}	-2.50	59380

Table 1: Global dissociation rates in pure oxygen

Several O_2 global dissociation rates were previously reported [29–33]. These data differ by the value of the pre-exponential and temperature dependence factors in the generalized Arrhenius form, shown in Table 1.

Another way to obtain state-specific dissociation rates is based on the Treanor-Marrone model [20]. The state-specific depletion rates are readily obtained by multiplying the global RC of dissociation by a nonequilibrium factor Z:

$$D_i^{O_2-O_2}\left(T, e_{v,i}\right) = Z\left(T, e_{v,i}\right) D^{O_2-O_2}\left(T\right), \tag{10}$$

where parameter Z is calculated as follows:

$$Z\left(T, e_{v,i}\right) = \frac{Q_v\left(T\right)}{Q_v\left(-U\right)} exp\left(\frac{e_{v,i}}{k_B}\left(\frac{1}{T}+\frac{1}{U}\right)\right), \tag{11}$$

where Q_v is the vibrational partition function, the adjustable parameter U is referred to as the "characteristic" dissociation temperature and should be chosen according to the best description of available data. A low value of U corresponds to the situation where quantum effects play an important role in dissociation, while infinite U means that dissociation is equally probable from any vibrational state. Several empirical values of U, such as $D/6k$, $D/3k$ and $3T$, have been suggested previously. In the present work a combination of them is chosen by comparing the dissociation rates generated in this way with the available O_2–O QCT data. Namely, in the present work, the parameter U is calculated as follows:

$$U = \frac{D_e}{6k}\left(1-\frac{e_{v,i}}{D_e}\right) + 3T\frac{e_{v,i}}{D_e}, \tag{12}$$

Equation (12) reflects the quantum behavior of the dissociation process for low lying vibrational states at low temperatures and an increase of depletion probability with temperature and for excited states. It was shown previously that the QCT data can be described more accurately using a variable Z-factor [34,35]. The comparison of D_i in O_2–O collisions, obtained from the Treanor-Marrone model with the O_2–O QCT data is shown in Fig. 1. One can see that the constant value $U = D/6k$ gives a strong underestimation of rates at high temperatures, where quantum effects are less pronounced. At the same time, the value of $U = 3T$ gives a strong underestimation of rates at low temperatures, which can be explained by the fact, that the "characteristic" dissociation temperature under these conditions is higher than $3T$. The hybrid value of these two values of U, given by Eq. (12), provides the best description of the O_2–O QCT data and is used in the present work to obtain the O_2–O_2 state-specific dissociation rates.

The O_2–O_2 state-specific dissociation rates, calculated by means of the Treanor-Marrone model for selected vibrational states from the global rates by Johnston, Park and Ibraguimova, are shown in Fig. 2. While the low-lying states have the conventional behavior of the dissociation RC, the result of the Treanor-Marrone model for highly excited states has a non-physical behavior, suggesting the decrease of dissociation RC at high temperatures. This decrease is larger for the larger absolute value of parameter B in Table 1. It is interesting to note, that in the work by [34] similar behavior was observed for N_2–N dissociation rates for $\nu \geq 60$, when compared to the results of the QCT method. Apparently, the choice of temperature dependence factor, B, plays an important role here. Those works, who report the larger absolute value of B, demonstrate the more significant decrease of D_i with temperature; this drop can be as large as two orders of magnitude in the temperature range between 1,000 and 10,000 K. In light of this finding, the present work adopts the O_2–O_2 global dissociation RC by [29], which has the smallest absolute value of B and was originally obtained with an emphasis on hypersonic temperatures. The comparison of scaled rates and those obtained by the Treanor-Marrone model for the O_2–O_2 system is shown in Fig. 3. The Treanor-Marrone

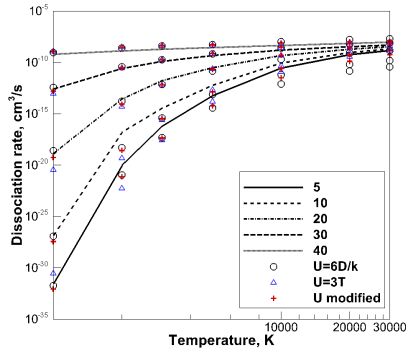

Fig. 1: O_2–O state-specific dissociation rates, QCT data and Eq. (12)

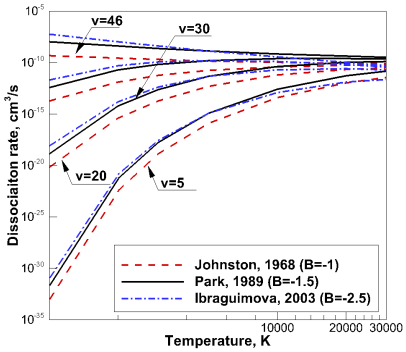

Fig. 2: O_2–O_2 state-specific dissociation rates, Eq. (12)

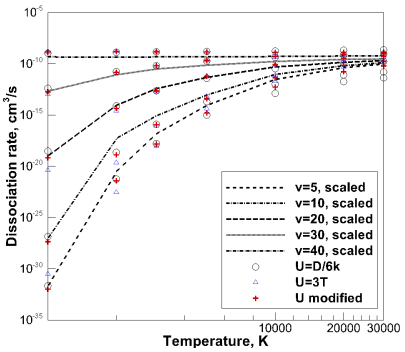

Fig. 3: O_2–O_2 state-specific dissociation rates, Eqs. (12) and (9)

rates, calculated using Eq. (12), again demonstrate the best agreement with the rates obtained by means of the scaling procedure, using Eq. (9).

Finally, it is possible to derive state-specific dissociation RCs from the QCT simulations using the six-dimensional O_4 PES obtained by the double many-body expansion method [36]. Although the complete calculation of RCs for all rovibrational states is expensive, the estimation of rotationally-averaged bound-free RCs appears to be tractable for several selected trans-rotational temperatures. Results of the QCT simulation using the Varandas O_4 PES for trans-rotational temperatures of 6000 and 10,000 K are given in Tables 2 and 3. Calculations are performed for selected low-lying as well for all highly excited vibrational states, since the latter are mainly responsible for dissociation during the QSS phase. The QCT data is compared to the O_2 (v)-O_2 BF RCs obtained by means of scaling procedure, Eq. (9) and by means of the Z factor approach, Eq. (11), that adopts the Camac global dissociation RC.

The QCT data for highly excited vibrational states is in good agreement with scaled state-specific RCs, underestimating the scaled RCs by a maximum of 20 %. On the other hand, the RCs obtained by means of the Z factor approach, are somewhat higher than the scaled state-specific RCs. Overall, the QCT and Z-factor RCs are different by a factor of two for vibrational states with $v > 40$. The situation for low-lying vibrational states is drastically different. These states are initially responsible for the generation of atomic oxygen immediately behind the shock wave, and their contribution is important under strongly nonequilibrium conditions, as will be shown later. For low vibrational states, the QCT, scaling and Z-factor approaches produce different results. The QCT method gives the highest BF RCs. The scaled RCs are lower than the QCT data by a factor of 2 to 3. The Z-factor approach generates state-specific RCs that are lower by more than an order of magnitude than the scaled RCs. In the present work, both scaled and Z-factor RCs are implemented in calculations, and the corresponding species number density is compared to the experimental data in Section III.E.

Vib. state	QCT, O_4 PES	Eq. (9), Camac	Eq. (11), $Z = D_e/6$, Camac
v=0	6.77×10^{-14}	1.49×10^{-14}	2.51×10^{-16}
v=10	1.71×10^{-12}	7.48×10^{-13}	6.95×10^{-14}
v=20	3.13×10^{-11}	1.65×10^{-11}	7.32×10^{-12}
v=30	2.34×10^{-10}	1.74×10^{-10}	2.30×10^{-10}
v=35	4.66×10^{-10}	4.18×10^{-10}	7.42×10^{-10}
v=40	7.43×10^{-10}	8.04×10^{-10}	1.54×10^{-9}
v=41	7.53×10^{-10}	8.87×10^{-10}	1.68×10^{-9}
v=42	1.04×10^{-9}	1.19×10^{-9}	1.80×10^{-9}
v=43	1.16×10^{-9}	1.36×10^{-9}	1.88×10^{-9}
v=44	1.33×10^{-9}	1.64×10^{-9}	1.93×10^{-9}

Table 2: State-specific O_2 (v)–O_2 dissociation RCs, cm^3/s, $T = T_r$=6000 K

Vib. state	QCT, O_4 PES	Eq. (9), Camac	Eq. (11), $Z = D_e/6$, Camac
v=0	3.97×10^{-12}	1.03×10^{-12}	1.27×10^{-14}
v=10	2.66×10^{-11}	1.13×10^{-11}	8.70×10^{-13}
v=20	8.47×10^{-11}	7.05×10^{-11}	2.87×10^{-11}
v=30	4.13×10^{-10}	2.82×10^{-10}	3.81×10^{-10}
v=35	6.57×10^{-10}	5.14×10^{-10}	9.21×10^{-10}
v=40	9.05×10^{-10}	8.45×10^{-10}	1.59×10^{-9}
v=41	9.34×10^{-10}	9.14×10^{-10}	1.70×10^{-9}
v=42	1.18×10^{-9}	1.18×10^{-9}	1.79×10^{-9}
v=43	1.25×10^{-9}	1.33×10^{-9}	1.85×10^{-9}
v=44	1.51×10^{-9}	1.59×10^{-9}	1.89×10^{-9}

Table 3: State-specific O_2 (v)–O_2 dissociation RCs, cm^3/s, $T = T_r$=10,000 K

The thermal equilibrium O_2–O_2 dissociation RC obtained by the QCT method is shown in Fig. 4 for a temperature range of 5000–10,000 K. This data is obtained by averaging state-specific RCs assuming $T_v = T_r = T$. The averaging of RCs over vibrational quantum number leads to the vanishing of differences observed in Table 2. The overall good agreement of the QCT global RC with the experimental data suggests that dissociation proceeds in a similar manner under thermal equilibrium conditions, however this fact has little application to the present study of nonequilibrium processes in shock flows.

D. Multi-temperature models

The SR approach becomes prohibitively expensive with increasing number of diatomic species and dimensionality of the problem. Although reduced order models that retain the main features of SR approach have been proposed recently [37], the MT models remain popular due to their simplicity. The solution of master equations provides new insight on parameters that are used in MT models. The present paper addresses the question of efficient utilization of the master equation results. The RVT MT model when formulated for a simple heat bath conditions consist of the following equations

$$\begin{cases} \dfrac{d}{dt}\left(\rho e_v\right) &= \rho_{O_2}\dfrac{e_v^\star - e_v}{\tau_v} + \dot{\omega}_{O_2} C_{DV} D_e, \\ \dfrac{d}{dt}\left(\rho e_r\right) &= \rho_{O_2}\dfrac{e_r^\star - e_r}{\tau_r} + \dot{\omega}_{O_2} C_{DR} D_e, \\ \dot{\omega}_{O_2} &= R\left(T_a\right) n_O^2 n_x - D\left(T_a\right) n_{O_2} n_x. \end{cases} \tag{13}$$

In Eq. 13, e_v and $e_v^\star$ are the O_2 vibrational energy evaluated at T_v and T, respectively, e_r and $e_r^\star$ are the O_2 rotational energy evaluated at T_r and T, respectively, ρ and ρ_{O_2} are the density of the O_2–O mixture and partial density of O_2, D_e is the classical dissociation energy, τ_v is the vibrational relaxation time, n_x is the projectile number density, in this particular case it is atomic oxygen. The global recombination RC, R , is estimated from D via the principle of detailed balance. Vibrational energy coupling coefficient, C_{DV} and C_{DR} coefficients correspond to the loss of vibrational and rotational energies normalized by the classical dissociation energy.

Vibrational and rotational relaxation times in O_2–O collisions were recently obtained on the accurate O_3 Varandas PES [10]. One should note that the vibrational relaxation time in the presence of rotational equilibrium is different than that when trans-rotational nonequilibrium is assumed. The latter τ_v is lower than the τ_v at $T = T_r$. This fact is taken into account in the present MT model.

The vibrational relaxation time in O_2–O_2 collisions was measured experimentally in multiple works [31, 38–41]. In the present work, recommendations on τ_v given in [30] are implemented. Because accurate state-specific transition RCs for the O_2–O_2 system are currently not available, vibrational relaxation times for VT and RVT MT models are assumed to be the same. For the same reason, the O_2–O_2 rotational relaxation time is derived from the approximation based on the experimental measurements at temperatures between 150 and 1300 K. The experimental data and the present approximation of rotational collisional number is shown in Fig. 5. The compilation of available experimental data is taken from [42].

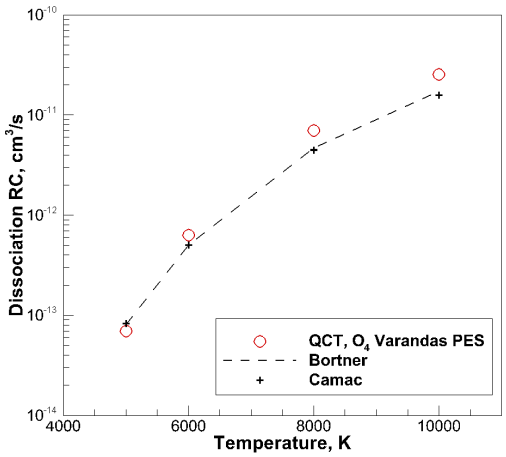

Fig. 4: Thermal equilibrium O_2–O_2 dissociation RC

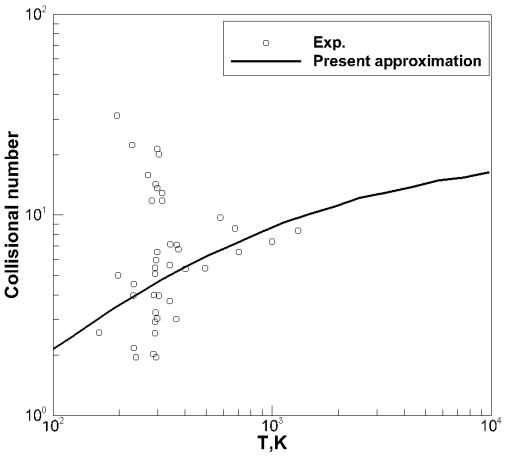

Fig. 5: O_2–O_2 rotational collisional number

One should discuss how the adjustable parameters, namely τ_v, τ_r, D, C_{DV} and C_{DR}, can be obtained from the system of master equations. The thermal relaxation times, when the complete set of state-specific RCs is available, are obtained by the e-folding method [43]. The dissociation RC, measured in shock tube experiments, should be referred to as the quasi-stationary dissociation RC. Vibrational thermalization at the moment of onset of dissociation is incomplete, and the QSS dissociation RC is lower than the RC estimated at thermal equilibrium conditions. Hence, it is necessary to re-evaluate the QSS dissociation RC as if the vibrational ladder is populated at $T_v = T$. According to Ref. [44], D^{QSS} and D^{eq} are related though the following empirical relation:

$$D^{QSS} = D^{eq} \frac{T}{T_v} exp\left(\frac{\tilde{D}}{RT}\left(\frac{1}{T} - \frac{1}{T_v}\right)\right), \tag{14}$$

where parameter $\tilde{D} = D_e - \beta RT$ describes the average loss of vibrational energy due to dissociation. The recommended range of β is between 1 and 2, in the present work β is set to 3/2.

The average loss of internal energy, C_{DV} and C_{DR}, is estimated as a product of the state-specific dissociation and recombination RCs and the instantaneous population of either the vibrational or rotational state [3]. The master equation approach generates time-dependent profiles of C_{DV} and C_{DR} that can be used to improve the accuracy of the conventional MT approach in which a constant value of these coefficients is assumed throughout the relaxation process.

For the description of shock tube experimental data, the conservation equations of mass, momentum and total energy must be added to Eq. (13). In the present work, these equations are formulated in the following manner:

$$\begin{cases} \dfrac{d}{dx}(\rho u) & = 0, \\ \dfrac{d}{dx}\left(p + \rho u^2\right) & = 0, \\ \dfrac{d}{dx}\left(h + \rho u^2/2\right) & = 0, \end{cases} \tag{15}$$

where u is the mean velocity of the flow, p is the total pressure, $h = \sum_s h^f_{0,s} r_s + 2.5RT \sum_s r_s + (e_r + e_v) r_{O_2}$ is the internal enthalpy of the flow, s is the species index, $h^f_{0,s}$ and r_s are the standard formation enthalpy and the molar concentration of species s. The conversion between time and spatial derivatives in Eqs. (13) and (15) is the following: $dx = u\, dt$. Since the original experimental data in [38] was reported for the laboratory system of coordinates, one needs to convert the time in this system of coordinates into the distance behind the shock wave: $x = \int V_{sh} dt_L$, where V_{sh} is the shock speed, t_L is the time in the laboratory coordinates system.

III. Results

A. Vibrational relaxation in O_2–O and O_2–O_2 collisions

The O_2–O vibrational relaxation time, previously obtained in [23] from the solution of master equations, is compared to the vibrational relaxation time derived from the monoquantum deactivation RC, reported by [9] and [45] in Fig. 7. The solid line describes the vibrational relaxation time by the VT model. The relaxation time, given by the short dashed line, is taken from experimental work [45]. The long dashed line represents the relaxation time derived from the monoquantum deactivation RC by [46]. The symboled line represents Park's curve fit to the Millikan-White (MW) equation [39] using the data by [4]. Theoretical calculations by [8] are shown by squares.

The vibrational relaxation time, obtained from the VT thermodynamic model, is in good agreement with the existing experimental data in the range from 1,000 K to 3600 K. The largest difference with Breen et al. data is observed in the high temperature region and is not higher than 15 %. Taking into account the overall uncertainty of shock tube facilities, the agreement with the experimental data is very satisfactory. To the authors' knowledge, other simulations that adopt a master equation, do not exist. The direct extrapolation of experimental data, performed by [30], suggests that the vibrational relaxation of oxygen by the parent atom becomes more efficient with temperature [30]. The present data supports the directly opposite temperature dependence: the vibrational relaxation time becomes smaller at low temperatures. This observation is in agreement with the results by [8]. The relaxation times, reported in [45], provide a good description of vibrational temperature behind shock waves in the range of temperatures from 4000 K to 10800 K. The agreement between results in [45] and those generated by the present VT model is very satisfactory and both results are substantially different from the MW relation. As pointed out in [23], the increase of O_2–O vibrational relaxation time with temperature is due to the barrierless O_3 PES. The energy randomization in the O_3 complex is especially efficient at low collision energies, while at high temperatures particles interact mostly via the repulsive part of potential.

The large attractive component in the O_3 potential energy surface has significant influence on the rates of mono- and multiquantum transitions as well. The rates of $v = 1 \to v' = 0$, $v = 10 \to v' = 9$ and $v = 10 \to v' = 5$ transitions for O_2–O and O_2–O_2 are shown in Fig. 8. For reference, the global dissociation RCs are also shown by dashed symboled lines. While the rates of O_2–O_2 bound-bound transitions demonstrate a strong temperature dependence, the O_2–O rates are nearly constant in the considered temperature range. Moreover, the O_2–O rates of multiquantum transitions are only slightly lower than that of a monoquantum jump. Also, the dissociation RC in collisions with oxygen radical is substantially higher than in O_2–O_2 and comparable to that of bound-bound transitions, which can be important in high temperature flow with an abundance of oxygen atoms. This subject is investigated in greater detail below.

The accuracy of O_2–O_2 VT and VV FHO RCs is an important subject in the present work. Unfortunately, rates obtained by trajectory simulation on an accurate PES are not available for temperatures relevant to hypersonic flows. However, the O_4 system was extensively studied at conditions corresponding to atmospheric chemistry [47–49]. The present FHO rates are compared with the available experimental and theoretical data in Fig. 6. Reactions of VT energy transfer $(O_2(v) + O_2 \to O_2(v-1) + O_2)$ and VV energy transfer $(O_2(v) + O_2(0) \to O_2(v-1) + O_2(1))$ are considered. Solid lines describe the present FHO data, long dashed lines correspond to rates by Coletti and Billing [48] and dashed-dotted line presents results by Campoz-Martínez et al. [49] Short dashed line gives the total (VT+VV) RC of energy removal based on the experimental measurements by Rogaski et al. [50] The difference in theoretical calculations by Coletti and Billing and Campoz-Martínez et al. is first of all due to the O_4 PES adopted for the calculations. The former work used a modified potential surface based on molecular beam experiments [47], where particles behave like rigid rotors. The work by Campoz-Martínez et al. used the PES by Varandas, obtained via the DMBE method. Unlike the former PES, the O_4 DBME PES introduces the open reaction channel for ozone formation. This particular fact leads to the appreciable difference in the VV RCs for high v [48]. The present VV+VT FHO RC has good agreement with the experimental data at $v > 20$. For low v, the agreement of the VT and VV FHO rates with those by Coletti and Billing is satisfactory.

The e-folding O_2–O_2 vibrational relaxation time is shown in Fig. 9 by the solid black line. The summary of experimental measurements, reflected in [30], is shown by square symbols. The present FHO rates satisfactorily describe the vibrational relaxation time in O_2–O_2 collisions in the considered temperature range as well as the deviation of relaxation time from the linear dependence at high temperatures due to the breakdown of the Landau-Teller theory.

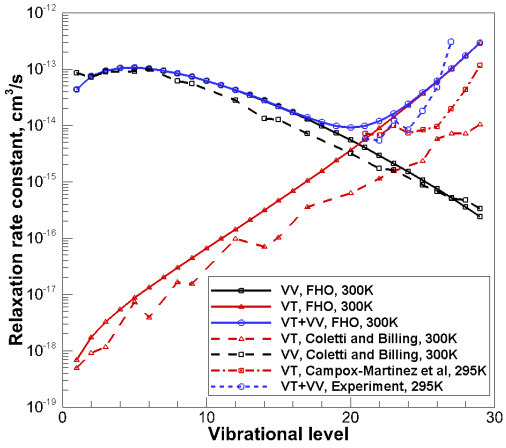

Fig. 6: VT and VV RCs at T = 300 K

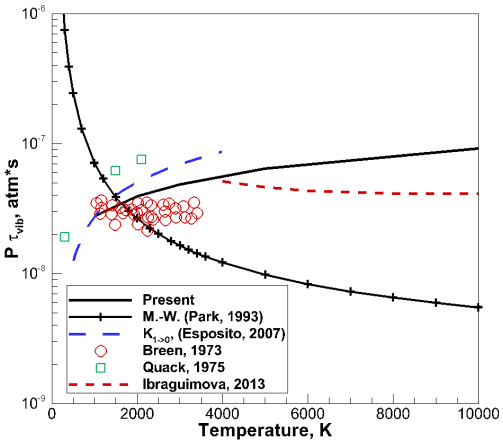

Fig. 7: O_2–O vibrational relaxation time

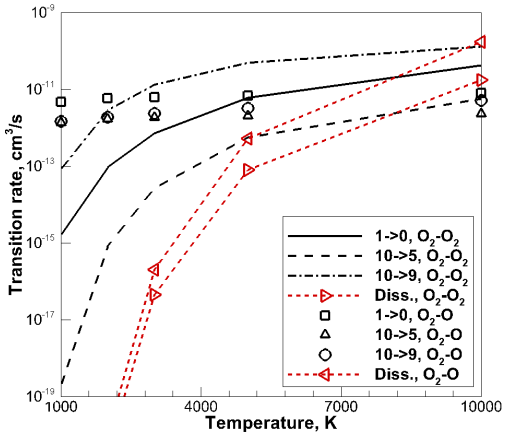

Fig. 8: O_2–O and O_2–Ar RCs of bound-bound and bound-free transitions

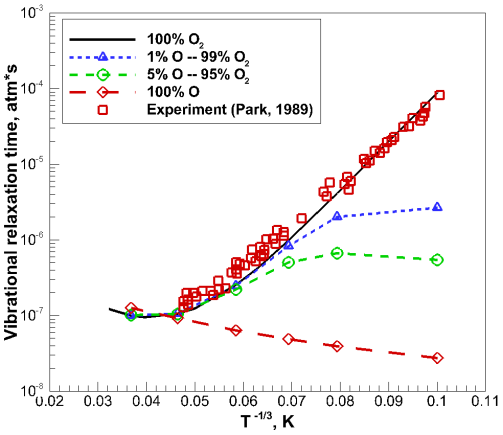

Fig. 9: E-folding vibrational relaxation time in various mixtures of O_2 and O species

The influence of a small concentration of atomic oxygen, admixed with the pure O_2, on vibrational relaxation time is shown in Fig. 9 with the short-dashed and long-dashed lines that correspond to 1 % and 5% molar fractions of atomic particles. The long-dashed line with diamond symbols corresponds to the vibrational relaxation time in O_2–O collisions. The presence of even a small concentration of atoms greatly reduces the relaxation time at moderate hypersonic temperates. This is the direct consequence of the anomalously fast vibrational energy randomization in ozone [8]. As temperature increases, the O_2–O relaxation becomes less efficient and the average relaxation time in the O_2–O mixture converges to the conventional MW dependence.

B. Multiquantum transitions

Existing kinetic theories, such as the FHO model, that are currently used to evaluate the probabilities of mono- and multiquantum transitions, predict the latter to be much smaller compared to that with $|\Delta v|$=1 at low and moderate temperatures, relevant to hypersonic flow. This result rests on the assumption of a strong repulsion between colliding particles that governs the trans-vibrational energy exchange. The probability of multiquantum transitions increases with temperature, nevertheless, for most practical applications the inclusion of transitions with $|\Delta v| \leq 5$ is usually enough to perform accurate SR simulations of shock flows [51]. However, because of the large attractive component in the O_3 potential energy surface, the probability of multi- and single quantum jumps in O_2–O collisions has the same order of magnitude, as can be seen in Fig. 8.

This section investigates the influence of transitions with $|\Delta v| > 1$ on the process of thermal relaxation.

The variation of the population of the vibrational ladder with time is shown in Figs. 10 and 11 for the cases of heating and cooling flows. The translational temperature is set to a constant value of 3,000 K. The initial vibrational temperature is set to 100 K and 10,000 K, respectively. The simulations are performed using the complete set of SR RCs as well as including transitions with $|\Delta v| \leq 5, 2$ and 1. The initial concentrations of atoms and molecules is set to 0.9×10^{18} and 0.1×10^{18} cm^{-3}. In both cases of heating and cooling flows, the multiquantum jumps play a significant role in the vibrational relaxation process. For the former, the influence of multiquantum jumps is more pronounced for the excited vibrational states due to the larger number of open relaxation channels. Specifically, for the lower vibrational states the multiquantum transitions result in the overpopulation and faster relaxation to equilibrium (v=5 and 10). For highly excited states, the multiquantum jumps have the opposite effect of faster depopulation (v=20 and 30). The influence of multiquantum transitions on the relaxation in the expanding flow is large for the entire vibrational ladder. In this case, failure to account for multiquantum jumps will lead to the underestimation of the population of ground and low-lying states and to the overestimation of the population of highly excited states.

The evolution of vibrational temperature to thermal equilibrium for the considered heat bath conditions is shown in Figs. 12 and 13 for translational temperatures of 3,000 and 10,000 K, respectively. The upper and lower parts of the plot correspond to the cooling and heating flows. Due to the fast vibrational relaxation and relatively slow dissociation at 3,000 K, the QSS state is reached only at the equilibrium temperature. In the case of T = 3,000 K the influence of multiquantum vibrational jumps is less pronounced in the heating flow due to the low population of excited states. However, for the expanding flow calculations with transitions $|\Delta v| \leq 5$ lead to a difference compared to those using the complete database. For both types of flows, the difference in the relaxation time and the duration of the QSS state between the full SR approach and the one with $|\Delta v| = 1$ is approximately one order of magnitude.

The variation of vibrational temperature with time in the case of T=10,000 K has a different pattern. Because in this case dissociation is faster, the nonequilibrium QSS state can be clearly observed in both types of flows. The QSS vibrational temperature and the duration of the QSS phase are similar for heating and shock flows. Since the initial concentration of atomic oxygen, set to 0.9×10^{18} cm^{-3}, is less than that in equilibrium, the QSS state is accompanied by strong dissociation, which leads to a drop of vibrational temperature below the translational one for the cooling flow, as can be seen in Fig. 13. Accounting for multiquantum jumps leads to a higher vibrational temperature and a shorter duration of the QSS phase.

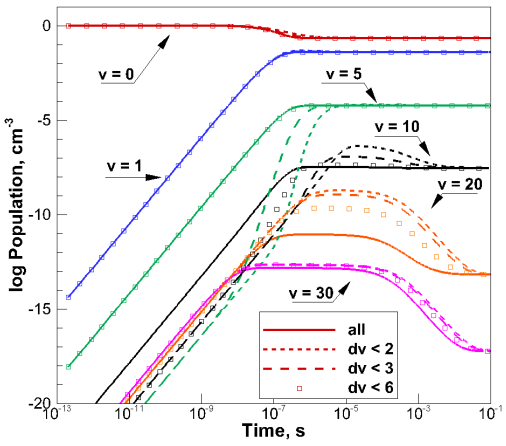

Fig. 10: Variation of the population of the vibrational ladder with time at T=3,000 K, heating flow

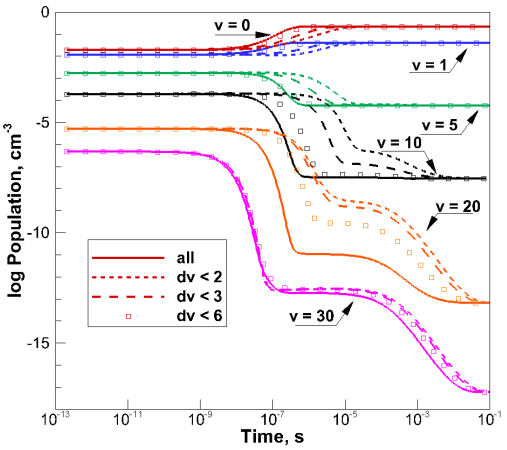

Fig. 11: Variation of the population of the vibrational ladder with time at T=3,000 K, cooling flow

C. Dissociation

Experimental measurements of dissociation rates in nitrogen [52] and oxygen [53] indicate that the depletion of gas proceeds more efficiently in the parent atom-diatom rather than in the diatom-diatom collisions. As pointed out in [54], one of the reasons for this is a "scrambling" effect of pre-collisional vibrational states

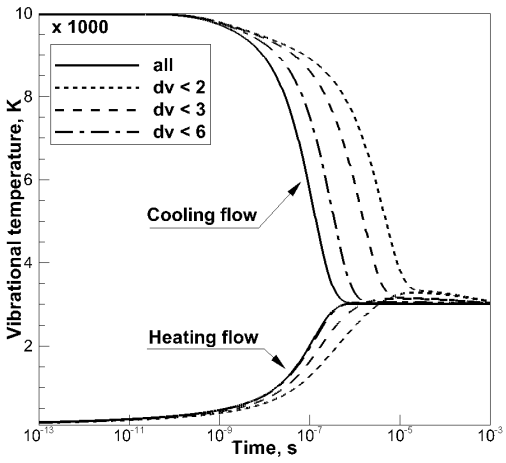

Fig. 12: Evolution of vibrational temperature with time under heating and cooling conditions, T=3,000 K, T_v^0=100 and 10,000 K

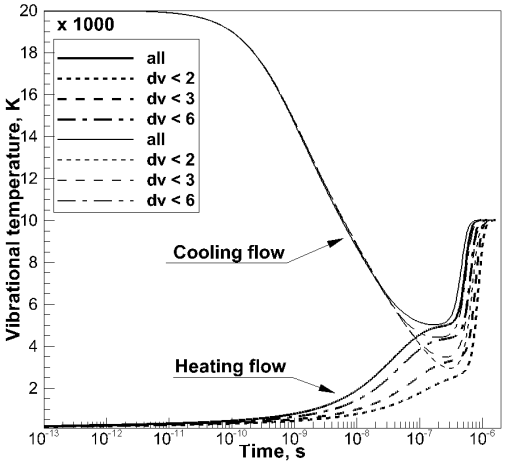

Fig. 13: Evolution of vibrational temperature with time under heating and cooling conditions, T=10,000 K, T_v^0=100 and 20,000 K

that takes place during the exchange reaction in N_2–N collisions. Because the insertion mechanism in the N_2–N system is more efficient than that in N_2–N_2, the former implicitly affects the populations of higher vibrational states that ultimately lead to dissociation.

It was recently shown [23] that the exchange reaction has a large impact on the energy randomization in the O_3 complex at collisions energies below 1 eV. Furthermore, the exchange mechanism is responsible for the large multiquantum jumps during the vibrationally inelastic collisions. Taking these facts into account, one can expect a large influence of oxygen radicals on not only the vibrational relaxation but also on the duration of the QSS phase. Presently adopted O_2–O and O_2–O_2 dissociation rates support the conclusions, made in [54]: the ratio of D^{O_2-O} and $D^{O_2-O_2}$ is equal to 3.90 at T=2,000 K, increasing up to 9.43 at T = 10,000 K. Thus, it is important to accurately model the amount of oxygen atoms in the flow and the population of the vibrational ladder prior to the QSS regime.

The evolution of vibrational temperature and species concentration with time is shown in Figs. 14 and 15 when only O_2–O and O_2–O_2 collisions are considered, respectively. In both cases the initial T_v is set to 100 K, and translational temperature is set to a constant in the range of 2,000 to 30,000 K. In the case of only atom-diatom collisions, the vibrational relaxation occurs mostly prior to the QSS phase at temperatures below 5,000 K, and the dissociation takes place from the vibrational ladder, populated at a nearly equilibrium temperature. As temperature increases further, the dissociation becomes faster, and the vibrational temperature during the QSS phase starts to deviate from the equilibrium value. Now, because the O_2–O vibrational relaxation time increases with temperature, unlike in O_2–O_2 collisions, and the dissociation rates follow the conventional Arrhenius form, the further increase of translational temperature does not lead to an increase of vibrational temperature during the QSS phase. The plateau, that is typically observed at low temperatures, is shorter and smeared. In other words, the increase of vibrational relaxation time with temperature in O_2–O collisions has a limiting effect on vibrational temperature during the QSS phase. One should use this observation with caution, because electronic excitation, that appears to be an additional channel of O_2–O collisions at high temperatures, is not included in the derivation of the present vibrational relaxation time.

Solutions of the master equations when only diatom-diatom collisions are considered are shown in Fig. 15. In contrast to the case with O_2–O relaxation, the vibrational temperature during the QSS phase increases monotonically in the considered interval of translational temperatures. The dissociation at temperatures not exceeding 5000 K occurs only after the vibrational relaxation is complete. This is true for both O_2 and O heat bath conditions. At higher temperatures, the depletion of molecules may occur prior to thermalization of the vibrational mode. At T=10,000 K nearly 20 % of O_2 is depleted in the case of a molecular heat bath. Under the same conditions of an atomic heat bath, the increase of n_O is comparable with that of the equilibrium composition. This is due to the faster dissociation in O_2-O collisions compared to the pure O_2

case. The separation of the QSS and relaxation phases is justified for the O_2–O system only at temperatures lower than 10,000 K.

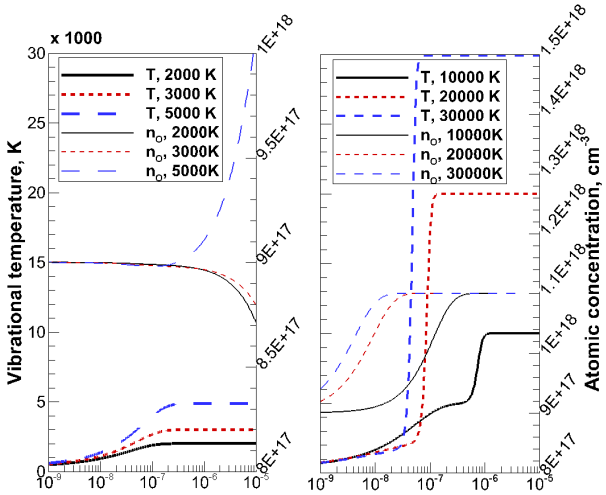

Fig. 14: Evolution of T_v and n_O with time, heat bath of oxygen atoms

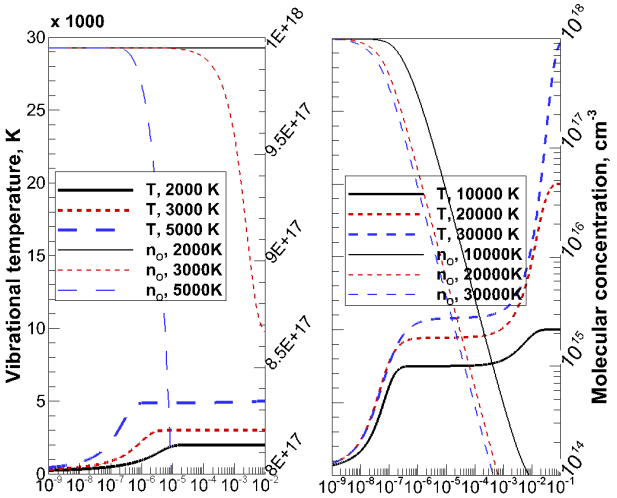

Fig. 15: Evolution of T_v and n_{O_2} with time, heat bath of oxygen molecules

The recombination process can be important in the nozzle flow with $T_v > T$ when the atomic concentration substantially exceeds the equilibrium composition. Because the population of the vibrational ladder exhibits a strongly non-Boltzmann dependence, the global rates of chemical reactions have a non-Arrhenius behavior. The multi-temperature model [30], popular due to its simplicity, is inadequate for describing the chemical composition in rapidly expanding flows for this reason. The system of master equations, coupled to the accurate rates of energy exchange in O_2–O_2 and O_2–O collisions, is an accurate tool for studying nonequilibrium kinetics in a strongly recombinative flow.

In the present paper, the nozzle flow kinetics is simulated at two initial vibrational temperatures of 3000 and 5000 K and at a fixed translational temperature of 1000 K. The initial molar fraction of atomic oxygen is set to 0.9. The evolution of vibrational population with time is shown in Fig. 16. In the case of lower T_v^0, the initial phase of thermal relaxation can be characterized by the formation of a long plateau above the initial distribution. This mechanism is attributed to a selective recombination to higher vibrational states. Because the excited states are strongly overpopulated, it is preferable to describe the rates of chemical transformation in terms of the population of the last vibrational state [18]. The lower vibrational states initially maintain a nearly constant population, while the extensive energy exchange takes place. For this reason, the dissociation RC, described by the vibrational temperature, would give misleading results in these simulations. The depopulation of lower states occurs only at the late stage of relaxation when the vibrational temperature of the system converges to the equilibrium value. It is worth to note that at stronger nonequilibrium conditions, $T_v^0 = 5000$ K, the up pumping of excited states does not occur, since those states are already densely populated. The formation of a plateau can be achieved by increasing the initial concentration of oxygen atoms.

D. Simulation of heat bath conditions

Due to the high cost of the SR approach there is a potential interest to use the information about nonequilibrium populations and state-specific rates in order to improve the accuracy of the simple and efficient MT approach. In the present work, the solution from the SR and MT models are compared side-by-side for ideal heat bath of oxygen at translational temperatures of 5000, 8000, 10,000 and 14,000 K. There are three primary parameters that can be adjusted in order to fit the solution of the MT approach to that of the SR method. Namely, these are the vibrational relaxation time, dissociation RC and the average loss of internal energy due to dissociation. It was shown recently [10] that the O_2–O e-folding relaxation time accurately describes the evolution of vibrational energy when incorporated in the Landau-Teller (LT) equation. Therefore, it is decided to keep the LT term and vibrational relaxation time unadjusted.

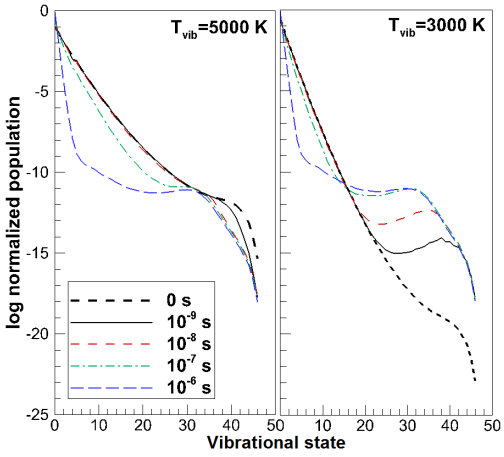

Fig. 16: Population of vibrational ladder in recombinative flow

The appropriate adjustment of dissociation RC and vibration-dissociation coupling parameter should be based on the temporal evolution of these parameters during thermalization. The dissociation RC and the vibration-dissociation coupling parameter are shown for considered heat bath conditions in Figs. 17 and 18. In Fig. 17, the symboled lines correspond to the instantaneous RC computed as the ratio of difference in the O_2 number density and the time step, dashed lines correspond to D^{QSS}. At low temperatures, the maximum of the instantaneous RC corresponds to the plateau at the QSS level. At higher temperatures, the QSS assumption breaks down and the QSS RC is bounded by some minimal and maximal values of instantaneous RC, shifting toward the lower bound with increasing temperature. In fact, the differences between minimum and maximum of instantaneous RC becomes smaller at higher temperatures. One should note that little to no dissociation occurs at low temperatures, hence it will be appropriate to assume the effective dissociation RC equal to QSS RC at these conditions. At higher temperatures, the dissociation occurs simultaneously with thermal relaxation, hence again, it will be accurate to assume the QSS RC as the replacement for the actual dissociation RC. The most pronounced inaccuracy in the modified MT model will be observed for intermediate temperatures.

Figure 18 illustrates that it is incorrect to assume a constant C_{DV} throughout the entire relaxation process. In fact, this coupling parameter has initially a very small value reaching a nearly constant level during the QSS phase and *thereafter*. For the sake of simplicity, a linear dependence of C_{DV} on T_v can be proposed:

$$C_{DV} = C_{DV}^{QSS} \times min\left(\frac{T_v}{T_v^{QSS}}, 1\right), \tag{16}$$

where C_{DV}^{QSS} and T_v^{QSS} are the vibration-dissociation coupling parameter and vibrational temperature during the QSS phase [10, 38]. The comparison of SR and modified MT approaches is shown in Fig. 19 for translational temperatures of 5000, 8000, 10,000 and 14,000 K. The adjusted MT approach performs very adequately, compared to the unadjusted MT model, presented in Ref. [10]. As expected, the least successful agreement is observed for moderate temperatures.

E. 1D shock flow simulation

Measurements of vibrational temperature of shock-heated oxygen was recently reported in the work by Ibraguimova et al. [38]. In these experiments, the absorption of laser radiation in O_2 Schumann-Runge bands was reported. The attenuation of radiation was analyzed using Beer's law and the tabulated absorption coefficients. The latter depends on vibrational and translational temperatures of the gas media and can be utilized specifically for the analysis of thermal nonequilibrium flows. By judging the amount of absorbed radiation, the O_2 vibrational temperature was derived in the range of translational temperatures between 4000 and 10800 K. The present work attempts to describe the results by Ibraguimova by utilizing the two- and three-temperature as well as the SR models of nonequilibrium shock flows.

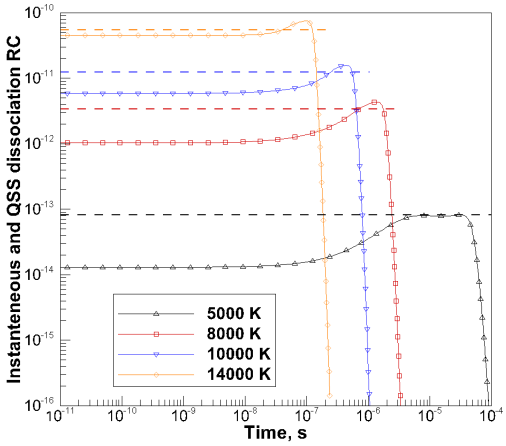

Fig. 17: O_2–O instantaneous and QSS dissociation RCs

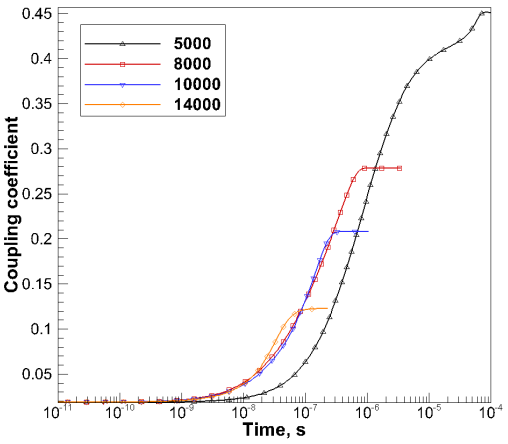

Fig. 18: O_2–O vibration-dissociation coupling parameter

A summary of the available experimental data is shown in Table 5. In the present work, six cases with different ambient pressure and shock velocity are studied. The pressure before the shock wave varies between 2 torr for mild nonequilibrium conditions and 0.8 torr for the strongest nonequilibrium experimental run. The velocity in the test runs varies from 3.07 to 4.44 km/s. Both measurements of translational and vibrational temperatures are available except the first, C1, case. For two cases with the strongest shock wave, the mass fraction of atomic oxygen is also reported.

The present work describes the experimental data by comparing the SR and multi-temperature models side-by-side for each case. Three variations of MT models are studied. The simplest one assumes the presence of trans-rotational equilibrium and adopts the Park vibrational relaxation times and dissociation RCs for O_2–O and O_2–O_2 collisions in the manner proposed in [30]. The Park model of governing temperature $T_a = \sqrt{TT_v}$ is used to simulate the effect of vibrational nonequilibrium on the dissociation RC. The Park correction of τ_v is used to modify the O_2–O_2 relaxation time, while O_2–O τ_v remains unchanged.

The modified VT MT model employs the QSS dissociation RC estimated at the translational temperature of the flow. The justification of such an approach to model nonequilibrium dissociation is given in the previous section. Additionally, the QCT O_2–O τ_v is adopted by the VT MT QSS model. This MT model assumes the presence of trans-rotational equilibrium as well.

The highest fidelity MT RVT QSS model, allows for rotational nonequilibrium and employs the RVT QSS O_2–O dissociation RC for describing the depletion in O_2–O collisions. A summary of the MT models is given in Table 4. To model rotational nonequilibrium, τ_r in O_2–O collisions is taken from the QCT calculations presented in [10]. The O_2–O_2 rotational relaxation time is calculated from the approximation of experimental data on rotational collisional number, shown in Fig. 5.

Model	O_2–O τ_v	O_2–O_2 τ_v	O_2–O τ_r	O_2–O_2 τ_r	O_2–O Diss.	O_2–O_2 Diss.	Noneq. coupling
MT VT Park	MW, [30]	MW, [30]	N/A	N/A	[30]	[30]	$T_a = \sqrt{TT_v}$, [30]
MT VT QSS	VT QCT	MW, [30]	N/A	N/A	VT QSS RC	[30]	VT QSS RC
MT RVT QSS	RVT QCT	MW, [30]	RVT QCT	Fig. 5	RVT QSS RC	[30]	RVT QSS RC

Table 4: Parameters of MT models

The SR models apply the FHO O_2–O_2 vibration-to-translation RCs, described in Section II. The O_2–O_2 dissociation RCs are obtained by means of the scaling procedure as well as applying the nonequilibrium factor Z given by Eq. 11. The comparison of vibrational and translational temperatures with the experimental data is performed using only O_2–O_2 dissociation RCs derived from the Z-factor approach. The species number density in C5 and C6 cases are computed using both scaled and Z-factor O_2–O_2 dissociation RCs.

The comparison with the experimental data starts from the case with the mildest shock. The distribution of translational, vibrational and rotational temperatures is shown in Figs. 20a–20b for case C1. The SR approach accurately captures the vibrational temperature prior to the dissociation as well as the point where

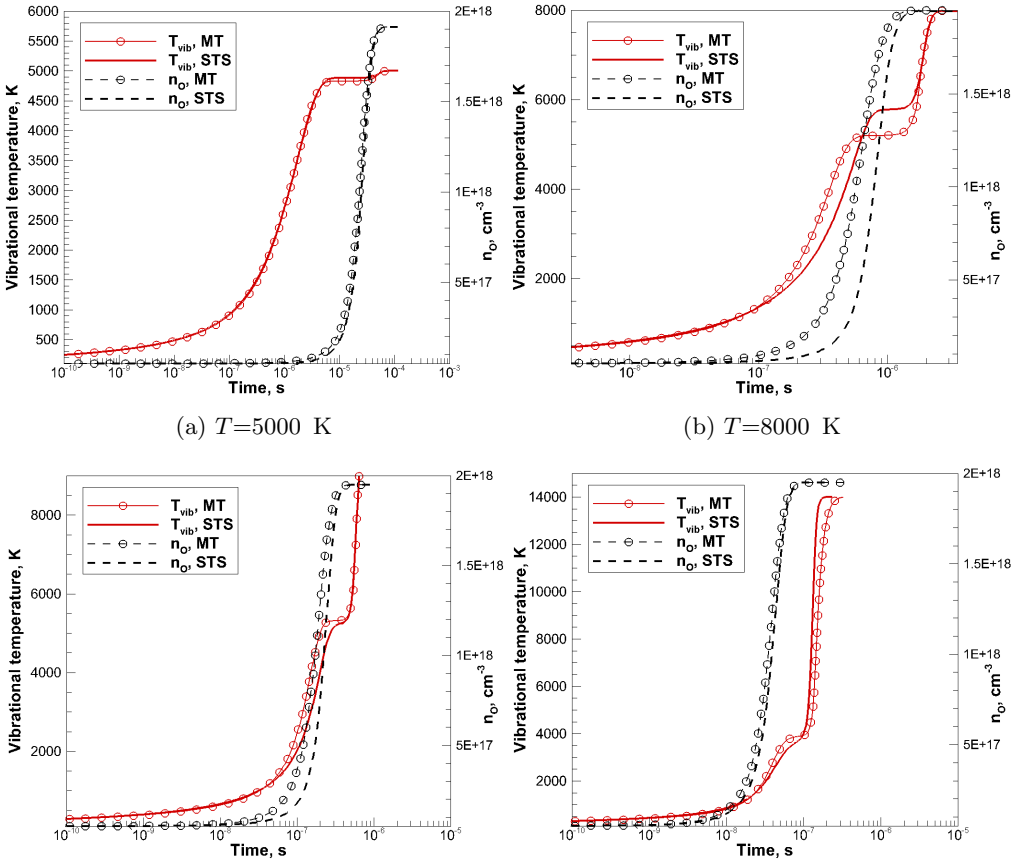

(a) T=5000 K (b) T=8000 K

(c) T=10,000 K (d) T=14,000 K

Fig. 19: Comparison of SR and modified MT approaches

Case	Pressure, torr	Velocity, km/s	Available T?	Available T_v?	Available Y_O?
C1	2.0	3.07	–	Yes	–
C2	1.0	3.40	Yes	Yes	–
C3	1.0	3.95	Yes	Yes	–
C4	1.0	4.132	Yes	Yes	–
C5	1.0	4.35	Yes	Yes	Yes
C6	0.8	4.44	Yes	Yes	Yes

Table 5: Summary of shock tube experiments [38]

T becomes equal to T_v. There is a subtle overestimation of the slope of T_v during the onset of dissociation by the SR model. This can be related to the uncertainty in O_2–O_2 state-specific dissociation RCs. The MT VT and RVT QSS models satisfactorily describe the vibrational relaxation phase, however the maximum of vibrational temperature is predicted less accurately than in the SR model. This is explained by the fact that the actual dissociation RC is smaller than the QSS RC prior to the phase of active dissociation, as follows from Fig. 17. The effect of rotational nonequilibrium is minimal at these translational temperatures.

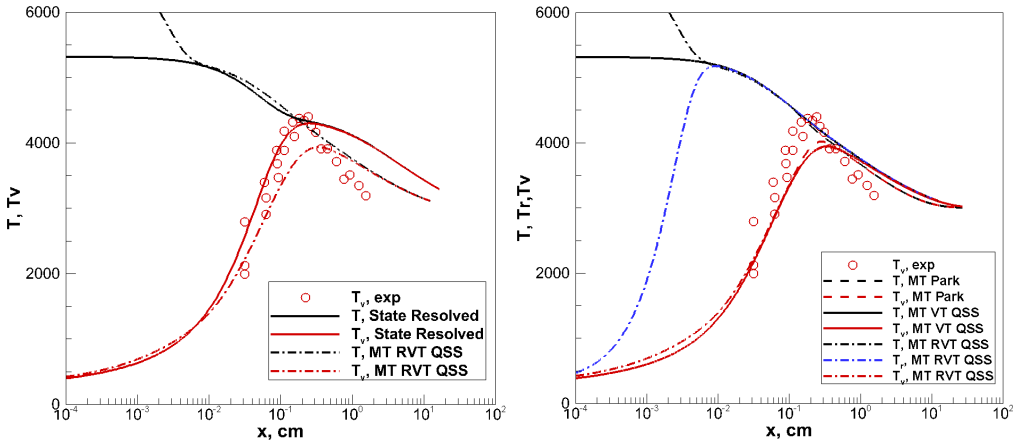

(a) State resolved and MT RVT QSS models (b) MT VT Park, MT VT QSS and MT RVT QSS models

Fig. 20: Translational, vibrational and rotational temperatures, C1

The results for the C2 - C4 cases, shown in Figs. 21a-23b, indicate that the SR approach is more accurate in describing the vibrational and translational temperatures than any of the MT models. This includes the description of vibrational and translational temperatures prior to the active dissociation, the peak of vibrational temperature and the width of vibrational nonequilibrium zone. The application of the QSS dissociation RC as the model of vibrational-dissociation coupling improves the agreement of vibrational temperature in MT QSS models compared to the MT VT Park model. The latter model appreciably underestimates the actual vibrational temperature during coupled vibration and dissociation thermalization.

Finally, for the strongly nonequilibrium C5-C6 cases, shown in Figs. 24a–25b, the SR approach demonstrates significantly more accurate prediction of post-shock vibrational and translational temperatures, compared to the Park MT model. These two cases can be characterized by a certain degree of rotational nonequilibrium. The rotational mode reaches equilibrium only two times faster than the vibrational mode. The trans-rotational nonequilibrium results in an increase of vibrational temperature in the zone of rotational nonequilibrium. This is explained by a lower QSS RC used in the RVT QSS model compared to that in the VT QSS model.

The accuracy of the considered models can also be assessed by comparing the mass fraction of atomic oxygen with the experimental data, as shown in Figs. 26a and 26b for the C5 and C6 cases, respectively. The black solid and dashed lines correspond to the SR model with O_2–O_2 dissociation RCs using nonequilibrium

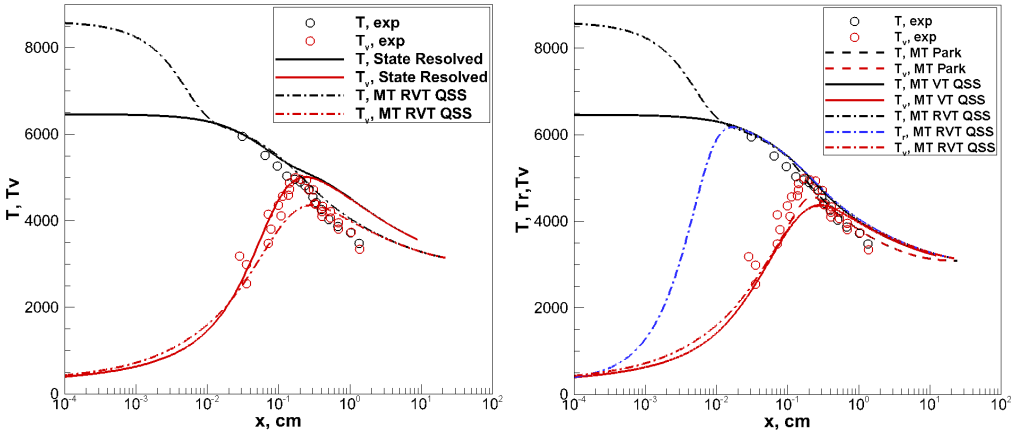

(a) State resolved and MT RVT QSS models (b) MT VT Park, MT VT QSS and MT RVT QSS models

Fig. 21: Translational, vibrational and rotational temperatures, C2

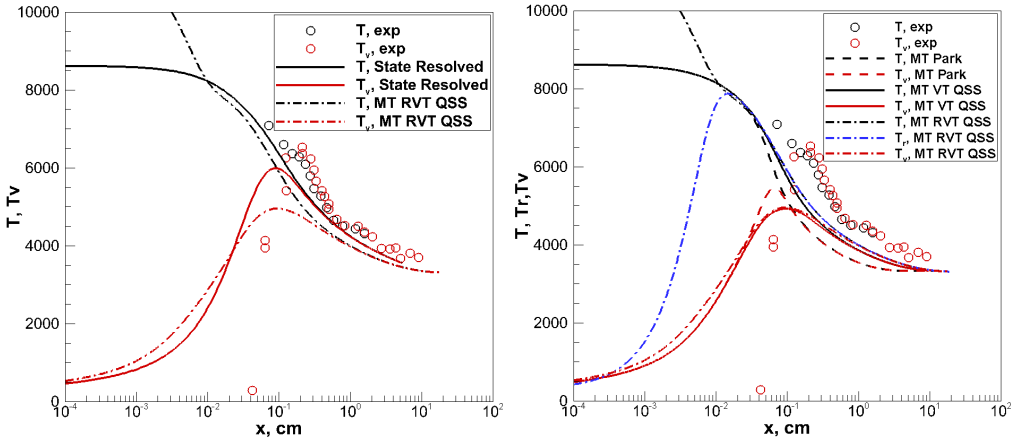

(a) State resolved and MT RVT QSS models (b) MT VT Park, MT VT QSS and MT RVT QSS models

Fig. 22: Translational, vibrational and rotational temperatures, C3

factor Z and scaling methods, respectively. It can be clearly seen that the approach based on the variable nonequilibrium factor produces a much slower accumulation of atomic oxygen compared to the approach with a constant scaling factor. This confirms the observation that immediately behind the shock wave the low lying vibrational states are responsible for initial generation of atomic oxygen. Because the Z-factor approach results in much lower O_2–O_2 bound-free RCs for $v < 10$ compared to other methods, this set of BF RCs gives the best agreement with the experimental data for the C5 and C6 cases. It is interesting to note that the implementation of the QSS VT and QSS RVT dissociation RCs provides a fairly good agreement between the MT model and the experimental data as well.

The vibrational temperature observed prior to the onset of dissociation (i.e. the maximum of T_v) is shown in Fig. 27. The horizontal scale corresponds to the maximum of translational temperature, measured immediately after the shock wave arrives at the optical station. In the entire range of nonequilibrium conditions, the present SR model accurately predicts the maximum of vibrational temperature. The leveling-off of T_v at strongly nonequilibrium conditions is captured as well. Unlike the SR model, the MT model underestimates the maximum of vibrational temperature. This observation is related to the fact that the governing temperature T_a, implemented in the MT VT Park model does not describe the population of

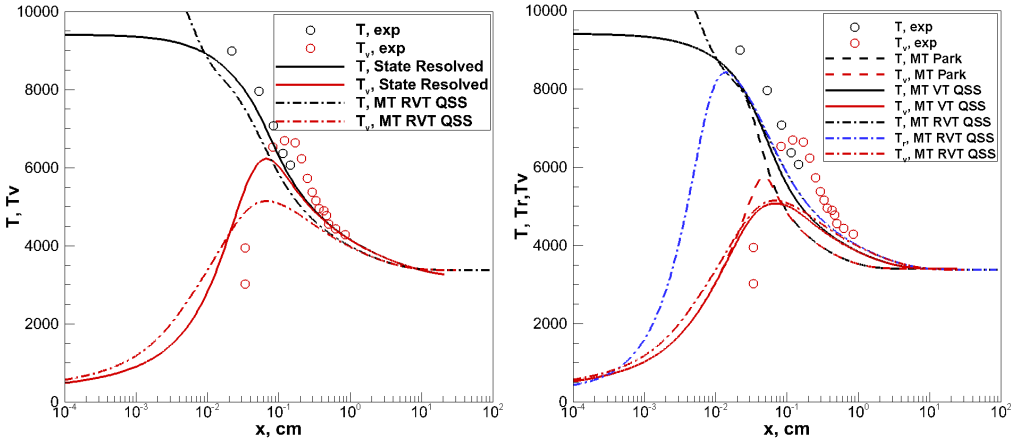

(a) State resolved and MT RVT QSS models (b) MT VT Park, MT VT QSS and MT RVT QSS models

Fig. 23: Translational, vibrational and rotational temperatures, C4

excited vibrational states, which is typically lower than the distribution of the vibrational ladder at thermal equilibrium conditions. Despite the good accuracy of the SR approach, it is highly desired in the future to repeat the present calculations with a complete set of $O_2\,(v)$–O_2 RCs generated on an accurate O_4 PES.

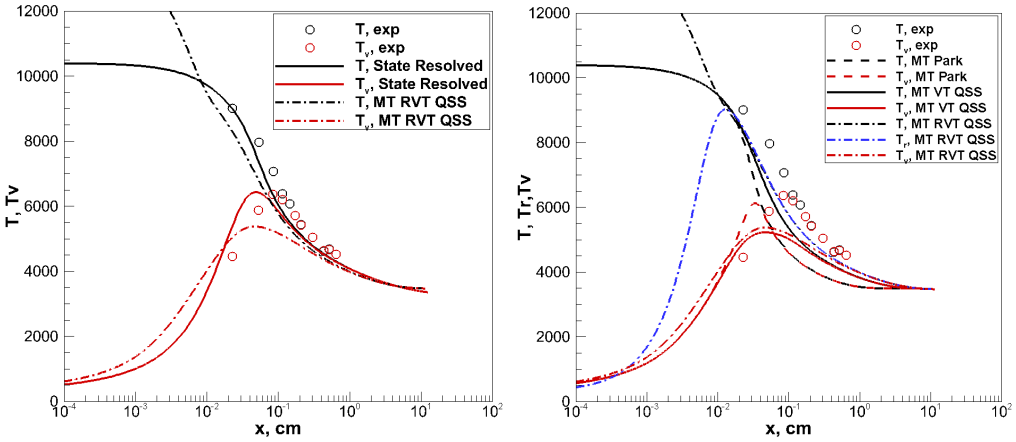

(a) State resolved and MT RVT QSS models (b) MT VT Park, MT VT QSS and MT RVT QSS models

Fig. 24: Translational, vibrational and rotational temperatures, C5

IV. Conclusion

Thermal relaxation and dissociation of molecular oxygen is studied by means of master equations and 1D shock flow in the presence of atom-molecule and bimolecular collisions. Accurate bound-bound and bound-free transition rates, generated by the QCT method, are adopted to model the O_2–O interaction. The FHO model is used to generate the VT and VV bimolecular relaxation rates. Both QCT and empirical approaches are used to obtain state-specific $O_2\,(v)$–O_2 dissociation RCs.

A strong dependence of vibrational relaxation time in the O_2–O mixture on the amount of atomic oxygen in the gas mixture is observed. The average relaxation time in the presence of a small (1-5% molar fraction) amount of oxygen atoms is several orders of magnitude lower than in pure oxygen at temperatures below 3,000 K. As temperature increases, this difference becomes smaller.

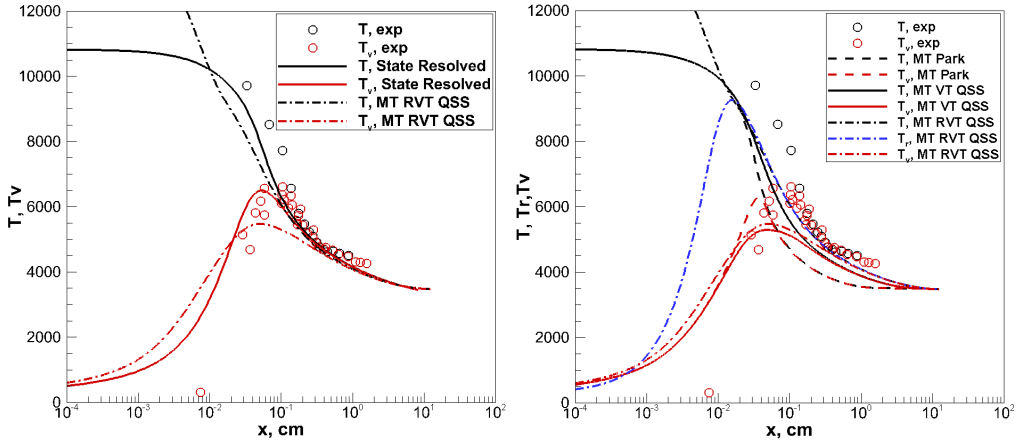

(a) State resolved and MT RVT QSS models (b) MT VT Park, MT VT QSS and MT RVT QSS models

Fig. 25: Translational, vibrational and rotational temperatures, C6

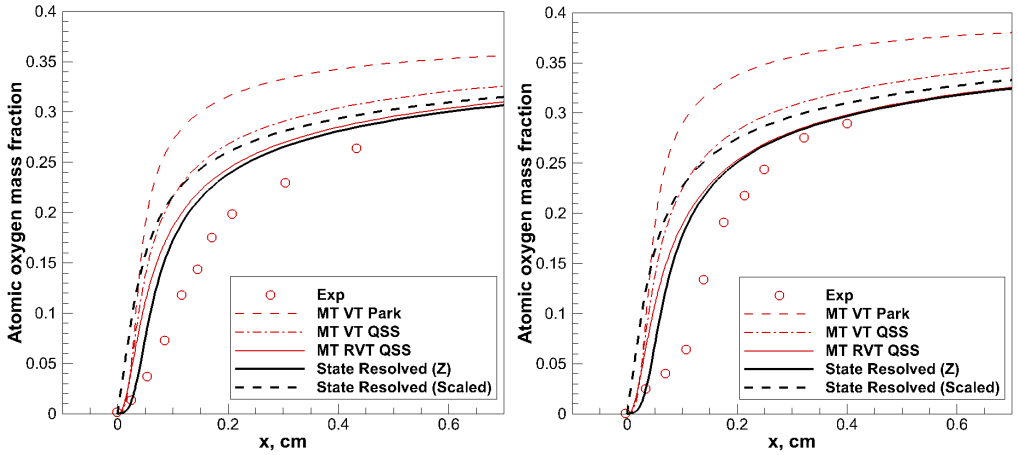

(a) C5 (b) C6

Fig. 26: Mass fraction of atomic oxygen

The efficient energy randomization in O_2–O collisions causes a strong over- and underpopulation of highly-excited vibrational states in heating and cooling flows, respectively. Moreover, the state-resolved populations are strongly defined by the multiquantum transitions. In the case of cooling flow, the multiquantum jumps noticeably affect even the population of the ground state. Failure to account for all possible transitions that take place during O_2–O collisions may lead to a strong overestimation of relaxation time in the gas mixture.

The present paper focuses on the accuracy of the multi-temperature models by implementing the newly generated QCT and master equation parameters in the low fidelity thermochemistry models. The study of heat bath conditions indicates that the O_2–O QSS dissociation RCs improves the accuracy of the MT model when implemented as the governing RCs without the traditional coupling of the translational and vibrational modes. At lower temperatures this approach is augmented by the fact that there is no to little dissociation prior to the QSS phase. At high temperatures, although there is a noticeable depletion at the early stage of relaxation, the instantaneous dissociation RCs change insignificantly and the constant QSS RC is well suited for describing the dissociation process.

Finally, a three temperature model is introduced for describing shock flows at translational temperatures between 4000 and 11000 K and compared to the state-resolved model and to the experimental data. Similarly to the simulations of heat bath conditions, the implementation of the QSS dissociation RCs leads to an

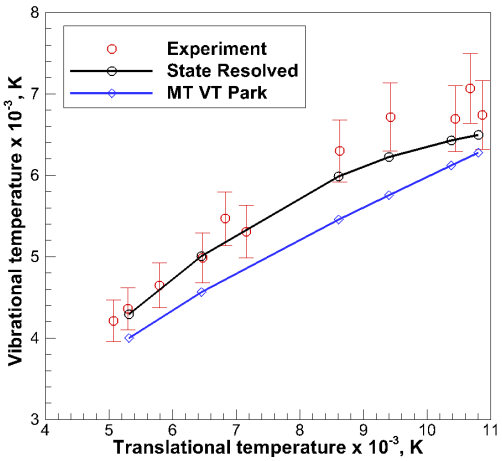

Fig. 27: Maximum of vibrational temperature behind the shock wave

improvement in the accuracy of the MT model, judging by the agreement of temperatures and species concentrations with the experimental data. However, due to unavailability of accurate O_2–O_2 RCs, the state-resolved models still appears to be more accurate. The state-specific O_2 (v)–O_2 dissociation RCs are important in describing the atomic oxygen number density under strongly nonequilibrium conditions. The empirical estimation of these coefficients using the nonequilibrium factor Z appears to be more accurate than the scaling procedure that is based on the O_2–O QCT data.

Acknowledgments

The authors gratefully acknowledge funding for this work through Air Force Office of Scientific Research Grant FA9550-12-1-0483. DA would like to thank Dr. Jae Gang Kim for the O_2–Ar QCT program code.

References

[1]Jaffe, R., Schwenke, D., and Chaban, G., "Theoretical analysis of N_2 collisional dissociation and rotation-vibration energy transfer," 47th AIAA Aerospace Sciences Meeting, AIAA Paper 2009-1569, Jan. 2009.

[2]Esposito, F., Capitelli, M., and Gorse, C., "Quasi-classical dynamics and vibrational kinetics of N+ N_2 (v) system," *Chemical Physics*, Vol. 257, No. 2, 2000, pp. 193–202.

[3]Panesi, M., Jaffe, R. L., Schwenke, D. W., and Magin, T. E., "Rovibrational internal energy transfer and dissociation of $N_2(^1\Sigma_g^+)$- $N(^4S_u)$ system in hypersonic flows," *The Journal of Chemical Physics*, Vol. 138, No. 4, 2013, pp. 044312.

[4]Kiefer, J. H. and Lutz, R. W., "The effect of oxygen atoms on the vibrational relaxation of oxygen," *Symposium (International) on Combustion*, Vol. 11, Elsevier, 1967, pp. 67–76.

[5]Breen, J., Quy, R., and Glass, G., "Vibrational relaxation of O_2 in the presence of atomic oxygen," *The Journal of Chemical Physics*, Vol. 59, No. 1, 1973, pp. 556–557.

[6]Kalogerakis, K. S., Copeland, R. A., and Slanger, T. G., "Measurement of the rate coefficient for collisional removal of O_2 ($X^3\Sigma_g^-$, v= 1) by O (^{3}P)," *The Journal of Chemical Physics*, Vol. 123, No. 19, 2005, pp. 194303.

[7]Lahankar, S. A., Zhang, J., Minton, T. K., Guo, H., and Lendvay, G., "Dynamics of the O-Atom Exchange Reaction $^{16}O(^3P)+ {}^{18}O^{18}O(^3\Sigma_g^-) \rightarrow {}^{16}O^{18}O\ (^3\Sigma_g^-)+ {}^{18}O\ (^3P)$ at Hyperthermal Energies," *The Journal of Physical Chemistry A*, 2016.

[8]Quack, M. and Troe, J., "Complex formation in reactive and inelastic scattering: Statistical adiabatic channel model of unimolecular processes III," *Berichte der Bunsengesellschaft für physikalische Chemie*, Vol. 79, No. 2, 1975, pp. 170–183.

[9]Esposito, F., Armenise, I., Capitta, G., and Capitelli, M., "O+O_2 state-to-state vibrational relaxation and dissociation rates based on quasiclassical calculations," *Chemical Physics*, Vol. 351, No. 1-3, 2008, pp. 91–98.

[10]Andrienko, D. A. and Boyd, I. D., "Rovibrational energy transfer and dissociation in O_2–O collisions," *The Journal of Chemical Physics*, Vol. 144, No. 10, 2016, pp. 104301.

[11]Varandas, A. and Pais, A., "A realistic double many-body expansion (DMBE) potential energy surface for ground-state O_3 from a multiproperty fit to ab initio calculations, and to experimental spectroscopic, inelastic scattering, and kinetic isotope thermal rate data," *Molecular Physics*, Vol. 65, No. 4, Nov 1988, pp. 843–860.

[12]Andrienko, D. A. and Boyd, I. D., "Master Equation Study of Vibrational and Rotational Relaxation of Oxygen," 45th AIAA Thermophysics Conference, AIAA Paper 2015-3252, June, 2015.

[13]Bruno, D., Capitelli, M., Esposito, F., Longo, S., and Minelli, P., "Direct Monte Carlo simulation of oxygen dissociation behind shock waves," 36th AIAA Thermophysics Conference, AIAA paper 2003-4059, June 2003.

[14]Dikalyuk, A., "Description of the vibrational relaxation process in O_2 heated by a shock wave using the state-to-state model," *Physical-Chemical Kinetics in Gas Dynamics*, Vol. 15, No. 2, 2014, pp. 1–7.

[15]Kewley, D., "Numerical study of anharmonic diatomic relaxation rates in shock waves and nozzles," *Journal of Physics B: Atomic and Molecular Physics*, Vol. 8, No. 15, 1975, pp. 2565.

[16]Armenise, I., Capitelli, M., and Gorse, C., "Nonequilibrium vibrational kinetics in the boundary layer of re-entering bodies," *Journal of Thermophysics and Heat Transfer*, Vol. 10, No. 3, 1996, pp. 397–405.

[17]Colonna, G., Armenise, I., Bruno, D., and Capitelli, M., "Reduction of state-to-state kinetics to macroscopic models in hypersonic flows," *Journal of Thermophysics and Heat Transfer*, Vol. 20, No. 3, 2006, pp. 477–486.

[18]Colonna, G., Pietanza, L. D., and Capitelli, M., "Recombination-assisted nitrogen dissociation rates under nonequilibrium conditions," *Journal of Thermophysics and Heat Transfer*, Vol. 22, No. 3, 2008, pp. 399–406.

[19]Adamovich, I. V., Macheret, S. O., Rich, J. W., and Treanor, C. E., "Vibrational energy transfer rates using a forced harmonic oscillator model," *Journal of Thermophysics and Heat Transfer*, Vol. 12, No. 1, 1998, pp. 57–65.

[20]Marrone, P. V. and Treanor, C. E., "Chemical relaxation with preferential dissociation from excited vibrational levels," *Physics of Fluids*, Vol. 6, No. 9, 1963, pp. 1215–1221.

[21]Truhlar, D. G. and Muckerman, J. T., "Reactive scattering cross sections III: quasiclassical and semiclassical methods," *Atom-Molecule Collision Theory*, Springer, 1979, pp. 505–566.

[22]Herzberg, G., *Molecular Spectra and Molecular Structure*, van Nostrand, 1957.

[23]Andrienko, D. and Boyd, I. D., "Investigation of Oxygen Vibrational Relaxation by Quasi-Classical Trajectory Method," *Chemical Physics*, Vol. 459, 2015, pp. 1–13.

[24]Gross, A. and Billing, G. D., "Isotope effects on the rate constants for the processes $O_2 + O \rightarrow O + O_2$ and $O_2 + O + Ar \rightarrow O_3 + Ar$ on a modified ground-state potential energy surface for ozone," *Chemical Physics*, Vol. 217, 1997, pp. 1–18.

[25]Nikitin, E., *Theory of elementary atomic and molecular processes in gases*, Oxford, Clarendon Press, 1974.

[26]Esposito, F. and Capitelli, M., "Quasiclassical trajectory calculations of vibrationally specific dissociation cross-sections and rate constants for the reaction $O + O_2 = 3O$," *Chemical Physics Letters*, Vol. 364, 2002, pp. 180–187.

[27]Andrienko, D. A. and Boyd, I. D., "Vibrational Relaxation and Dissociation of Oxygen in Molecule-Atom Collisions," 45th AIAA Thermophysics Conference, AIAA paper 2015-3251, June 2015.

[28]Steele, D., Lippincott, E. R., and Vanderslice, J. T., "Comparative study of empirical internuclear potential functions," *Reviews of Modern Physics*, Vol. 34, No. 2, 1962, pp. 239.

[29]Bortner, M., "A Review of Rate Constants of Selected Reactions of Interest in Re-Entry Flow Fields in the Atmosphere. Tech," Tech. rep., Note 484, Nat. Bur. Standards, US Dep. Com, 1969.

[30]Park, C., "Review of chemical-kinetic problems of future NASA missions. I - Earth entries," *Journal of Thermophysics and Heat Transfer*, Vol. 7, No. 3, 1993, pp. 385–398.

[31]Camac, M., "O_2 Vibration Relaxation in Oxygen-Argon Mixtures," *Journal of Chemical Physics*, Vol. 34, No. 2, 1961, pp. 448–459.

[32]Ibraguimova, L., Smekhov, G., and Shatalov, O., "Recommended rate constants of chemical reactions in an H_2-O_2 gas mixture with electronically excited species $O_2(\Delta)$, O(D), $OH(^2\Sigma)$ involved," *Physical-Chemical Kinetics in Gas Dynamics*, Vol. 1, 2003, pp. 1–31.

[33]Johnston, H. S., "Gas phase reaction kinetics of neutral oxygen species," Tech. Rep. NSRDS-NBS 20, NASA, 1968.

[34]Capitelli, M., Esposito, F., Kustova, E., and Nagnibeda, E., "Rate coefficients for the reaction $N_2(i) + N = 3N$: a comparison of trajectory calculations and the Treanor–Marrone model," *Chemical Physics Letters*, Vol. 330, No. 1, 2000, pp. 207–211.

[35]Kustova, E., Nagnibeda, E., Oblapenko, G., Savelev, A., and Sharafutdinov, I., "Advanced models for vibrational–chemical coupling in multi-temperature flows," *Chemical Physics*, Vol. 464, 2016, pp. 1–13.

[36]Varandas, A. and Pais, A., "Double Many-Body Expansion Potential Energy Surface for $O_4(^3A)$, Dynamics of the $O(^3P) + O_3(^1A_1)$ reaction, and Second Virial Coefficients of Molecular Oxygen," *Theoretical and Computational Models for Organic Chemistry*, Springer, 1991, pp. 55–78.

[37]Panesi, M. and Lani, A., "Collisional radiative coarse-grain model for ionization in air," *Physics of Fluids (1994-present)*, Vol. 25, No. 5, 2013, pp. 057101.

[38]Ibraguimova, L., Sergievskaya, A., Levashov, V. Y., Shatalov, O., Tunik, Y. V., and Zabelinskii, I., "Investigation of oxygen dissociation and vibrational relaxation at temperatures 4000–10 800 K," *Journal of Chemical Physics*, Vol. 139, No. 3, 2013, pp. 034317.

[39]Millikan, R. C. and White, D. R., "Systematics of vibrational relaxation," *The Journal of Chemical Physics*, Vol. 39, No. 12, 1963, pp. 3209–3213.

[40]Generalov, N. and Losev, S., "Vibrational Exitation and Decomposition of Molecular Oxygen and Carbon Dioxide Behind Shock Waves," *Journal of Quantum Spectroscopy and Radiative Transfer*, Vol. 6, 1966, pp. 101–125.

[41]Blackman, V. H., *Vibrational relaxation in oxygen and nitrogen*, Ph.D. thesis, Cambridge Univ Press, 1955.

[42]Capitelli, M., Ferreira, C. M., Osipov, A. I., and Gordiets, B. F., *Plasma kinetics in atmospheric gases*, Springer, 2000.

[43]Park, C., "Rotational relaxation of N_2 behind a strong shock wave," *Journal of Thermophysics and Heat Transfer*, Vol. 18, No. 4, 2004, pp. 527–533.

[44]Shatalov, O., "Molecular dissociation of oxygen in the absence of vibrational equilibrium," *Combustion, Explosion, and Shock Waves*, Vol. 9, No. 5, 1973, pp. 610–613.

[45]Ibraguimova, L., Sergievskaya, A., and Shatalov, O., "Dissociation rate constants for oxygen at temperatures up to 11000 K," *Fluid Dynamics*, Vol. 48, No. 4, 2013, pp. 550–555.

[46]Esposito, F. and Capitelli, M., "The relaxation of vibrationally excited O_2 molecules by atomic oxygen," *Chemical Physics Letters*, Vol. 443, No. 4, 2007, pp. 222–226.

[47]Aquilanti, V., Ascenzi, D., Bartolomei, M., Cappelletti, D., Cavalli, S., de Castro Vitores, M., and Pirani, F., "Molecular Beam Scattering of Aligned Oxygen Molecules. The Nature of the Bond in the O_2-O_2 Dimer," *Journal of the American Chemical Society*, Vol. 121, No. 46, 1999, pp. 10794–10802.

[48]Coletti, C. and Billing, G. D., "Vibrational energy transfer in molecular oxygen collisions," *Chemical Physics Letters*, Vol. 356, No. 1, 2002, pp. 14–22.

[49]Campos-Martınez, J., Carmona-Novillo, E., Echave, J., Hernández, M. I., Hernández-Lamoneda, R., and Palma, J., "Jump in depletion rates of highly excited O_2: reaction or enhanced vibrational relaxation?" *Chemical Physics Letters*, Vol. 289, No. 1, 1998, pp. 150–155.

[50]Rogaski, C., Mack, J., and Wodtke, A., "State-to-state rate constants for relaxation of highly vibrationally excited O_2 and implications for its atmospheric fate," *Faraday Discussions*, Vol. 100, 1995, pp. 229–251.

[51]Neitzel, K., Kim, J. G., and Boyd, I. D., "Nonequilibrium Modeling of Oxygen in Reflected Shock Tube Flows," *11th AIAA/ASME Joint Thermophysics and Heat Transfer Conference*, AIAA paper 2014-2961, June 2014, 2014.

[52]Byron, S., "Shock-Tube Measurement of the Rate of Dissociation of Nitrogen," *The Journal of Chemical Physics*, Vol. 44, No. 4, 1966, pp. 1378–1388.

[53]Baulch, D., Cobos, C., Cox, R., Esser, C., Frank, P., Just, T., Kerr, J., Pilling, M., Troe, J., Walker, R., et al., "Evaluated kinetic data for combustion modelling," *Journal of Physical and Chemical Reference Data*, Vol. 21, No. 3, 1992, pp. 411–734.

[54]Valentini, P., Schwartzentruber, T. E., Bender, J. D., Nompelis, I., and Candler, G. V., "Direct simulation of rovibrational excitation and dissociation in molecular nitrogen using an ab initio potential energy surface," 45th AIAA Thermophysics Conference, AIAA Paper 2015-474, June, 2015.